Accepted Manuscript

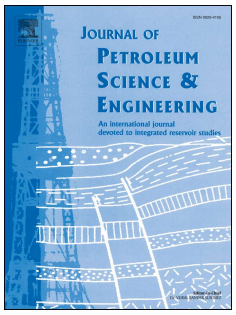

Development of a multi-continuum quadruple porosity model to estimate CO_2 storage capacity and CO_2 enhanced shale gas recovery

Minglu Wu, Mingcai Ding, Jun Yao, Chenfeng Li, Xuan Li, Jiamin Zhu

PII: S0920-4105(19)30315-8

DOI: https://doi.org/10.1016/j.petrol.2019.03.077

Reference: PETROL 5927

To appear in: *Journal of Petroleum Science and Engineering*

Received Date: 9 December 2018

Revised Date: 2 March 2019

Accepted Date: 28 March 2019

Please cite this article as: Wu, M., Ding, M., Yao, J., Li, C., Li, X., Zhu, J., Development of a multi-continuum quadruple porosity model to estimate CO_2 storage capacity and CO_2 enhanced shale gas recovery, *Journal of Petroleum Science and Engineering* (2019), doi: https://doi.org/10.1016/j.petrol.2019.03.077.

Development of a multi-continuum quadruple porosity model to estimate CO_2 storage capacity and CO_2 enhanced shale gas recovery

Minglu Wu*[a], Mingcai Ding[b], Jun Yao[a], Chenfeng Li[c], Xuan Li[a], Jiamin Zhu[a]

[a] *School of Petroleum Engineering in China University of Petroleum, Qingdao 266580, China.*

[b] *School of Mathematics in Dalian University of Technology, Dalian 116024, China.*

[c] *College of engineering in Swansea University Bay Campus, Swansea SA1 8EN, UK.*

Abstract

Geologic storage of CO_2 in shale formation not only enhances natural gas recovery, but also sequestrates CO_2 effectively. According to this technology, a multi-continuum quadruple porosity binary component gas model is developed to investigate carbon dioxide storage capacity and CO_2 enhanced shale gas recovery, which is based on multiple flow mechanisms, including dissolution, adsorption/desorption, viscous flow, diffusion, slip flow and stress sensitivity of hydraulic fractures. This fully coupled model is divided into quadruple media, including organic matters, organic pore system, matrix system and natural fracture system. The matrix-fracture transfer flow is simulated by modified multiple interacting continua (MINC) method. Embedded discreate fracture model (EDFM) is introduced to describe the gas flow in hydraulic fractures and the transfer flow between hydraulic fractures and natural fractures. Finite difference method (FDM) and quasi-Newton iterative method are applied to solve this model. The reliability and practicability of this model is validated by matching the production history of a fractured horizontal well in shale gas reservoir. The effects of relevant parameters on production curves are analyzed, including adsorption parameters, dissolution parameters, well production pressure, injection pressure, volumetric fraction of kerogen and injection opportunity. The result shows that the model in this work is reliable and practicable, and the model presented here can be used to investigate the injectivity of CO_2 and CO_2 enhanced shale gas recovery.

Keywords: CO_2 storage; enhanced shale gas recovery; multiple flow mechanisms; quadruple porosity model; fractured horizontal well

1. Introduction

Shale gas is one of unconventional resources, its economic and efficient development can effectively meet people's demand for clean energy and solve the current energy shortage problem. Due to ultra-low permeability of shale formation, shale gas is hard to be exploited by conventional technologies, so that horizontal drilling and formation fracturing techniques were used to exploit shale gas. The induced fractures created by the fracturing increase the shale permeability around the horizontal well and improve the final shale gas cumulative production (Wu, Moridis et al. 2009, He, Teng et al. 2016, Wu, Ding et al. 2017).

According to previous studies, shale gas stores at different pores, which include organics or bitumen with dissolved gas(Javadpour, Fisher et al. 2007, Javadpour 2009), the surface of kerogen and clays with adsorbed gas(Liu, Xiao et al. 2015, He, Teng et al. 2016), matrix pores and natural fractures with free gas. Porous kerogen, with huge specific surface area, has been proved to be

ideal storage space for shale gas, and gas in kerogen mainly composed of free gas in organic pores, adsorbed gas on the wall of kerogen bulk and dissolved gas in organic matter. However, the dissolution of kerogen is usually neglected in most models for shale gas reservoir. In fact, the dissolution capacity of bitumen and organics has been proved to be quite considerable(Svrcek and Mehrotra 1982, Swami and Settari 2012). The solubility coefficient of CH_4 in bitumen of kerogen can reach up to 1.43×10^{-6} $m^3/Pa/m^3$ and the diffusion coefficient of dissolved gas in in organics can arrive at $10^{-20}m^2/s$(He, Teng et al. 2016). Therefore, dissolution of gas in shale gas reservoir cannot be ignored. Due to the complex pore structure and unique gas storage mode, the flow of gas in the shale formation follows multiple mechanisms, including adsorption/desorption, dissolution, diffusion, slip flow and viscous flow(He, Teng et al. 2016). During horizontal well production, the free gas in natural fractures and hydraulic fractures comes out first, and follows the slip flow and viscous flow. Then the free gas in matrix pores transfer into natural fractures. And then the adsorbed gas desorbs from the surface of organics and inorganics when the pressure falls below adsorption pressure. Lastly, the dissolved gas in organic matter diffuses into kerogen pores when pressure drops, on the contrary, gas dissolves in organic matter if pressure rises.

In another hand, CO_2 capture and storage (CCS) is regarded as a promising method to cut down CO_2 emissions, which can lighten global warming significantly. Geologic storage of CO_2 in shale formation is one of feasible options to sequestrate CO_2, which can reduce the CCS costs by using the facilities for shale gas exploitation. Moreover, injectivity of CO_2 into shale formation can enhance shale gas recovery, which is mainly due to the following three reasons. Firstly, the injection of CO_2 allows the formation to be re-pressurized with the injected gas, which can promote the flow ability of natural gas. In addition, CO_2 displaces CH_4 since the shale has a stronger affinity for carbon dioxide than for methane during competitive absorption between CO_2 and CH_4(Kang, Fathi et al. 2011, Sun, Yao et al. 2013, Heller and Zoback 2014, Edwards, Celia et al. 2015, Gallo and Carballo 2016). The experimental results of Kang, Fathi et al. (2011) show that the amount of CO_2 adsorption was five to ten times greater than the amount of CH_4 adsorption in the same gas shale. Lastly, carbon dioxide in shale formation not only stored in free and adsorbed state, but also can be dissolved in organic matters(Svrcek and Mehrotra 1982, Swami and Settari 2012), which leads to more dissolved natural gas displaces from organic matter by CO_2. Therefore, it is significant to investigate the storage capacity of CO_2 and CO_2 enhanced natural gas recovery. However, accurate reservoir simulation of shale gas mining and CO_2 storage is very difficult due to the ultra-low permeability, complex pore structure, multiple storage mode and multiple flow mechanisms.

In order to investigate the injectivity of CO_2 and CO_2 enhanced shale gas recovery, many semi-analytical and numerical models were proposed. The semi-analytical models, based on source function, can solved the pressure and rate solution efficiently. The previous studies (Chen, Liao et al. 2015, Gallo and Carballo 2016, Xiao, Tian et al. 2016) introduced pressure transient analysis (PTA) and rate transient analysis (RTA) to estimate the storage capacity of CO_2 in depleted shale gas reservoir. However, these semi-analytical models have far more limitations when they are used to simulate geologic storage of CO_2 in shale formation, the main reasons are as follows. In one hand, numerous simplifications were made in these models to solve the strong nonlinear equations, which enlarges the error between the calculated result and the real data. In another hand, the storage of carbon dioxide in shale reservoirs contains lots of complex mechanisms, including multiple component flow, porous flow, competitive absorption and

dynamic operation of wells. Thus, it is difficult to use these semi-analytical models to investigate the injectivity of CO_2 into shale gas reservoir.

In recent years, numerous multiple component numerical models (Sun, Yao et al. 2013, Jiang, Shao et al. 2014, Boosari, Aybar et al. 2015, Edwards, Celia et al. 2015, Merey and Sinayuc 2016, Kim, Cho et al. 2017, Xu, Zeng et al. 2017)were established to simulate the storage of CO_2 in shale gas reservoirs. Sun, Yao et al. (2013) proposed a dual-porosity model to investigate the CO_2 sequestration in shale gas reservoirs, in which, multiple binary gas transport mechanisms, including viscous flow, Knudsen diffusion and ordinary diffusion, were considered. However, the multiple fractured horizontal well, as the only effective exploration way can be used now in most ultra-low permeability shale gas reservoirs, has not been used to study enhancement of natural gas recovery or injectivity of CO_2 in their model. Jiang, Shao et al. (2014) developed a multi-continuum multi-component simulator to investigate CO_2 storage in shale gas reservoirs, which incorporates multiple mechanisms and considers the complex fracture network around the fractured horizontal well in shale reservoirs. Multiple interacting continua (MINC) method was applied to simulate the fluid migration between matrix and natural fractures, in addition, embedded discrete fracture model (EDFM) was used to describe the flow in hydraulic fractures the transfer flow between hydraulic fractures and MINC elements. However, the dissolution of CO_2 and CH_4 in organic matter was ignored in their model, which is one of important storage modes in shale gas reservoirs as discussed above. Moreover, they haven't considered the fluid flow in stimulated reservoir volume (SRV) around fractured horizontal well, which has been proved to be very important to improve final cumulative gas production and recovery of fractured shale gas reservoirs. Edwards, Celia et al. (2015) established a one-dimension linear flow model to estimate CO_2 injection and storage capacity for geological sequestration in shale gas reservoirs, and excess adsorption of CO_2 and CH_4 was considered. Obviously, it's difficult to use one-dimension linear flow model to describe the fluid migration in shale formation with complex pore structure. Xu, Zeng et al. (2017) proposed a triple-porosity dual permeability model to assess the feasibility of CO_2 enhanced shale gas recovery and CO_2 storage capacity, which considering binary component and multiple flow mechanism. However, dissolution of organic matter and SRV were also ignored in their study.

In light of the questions discussed above, this paper presented a fully coupled multi-continuum quadruple porosity binary component gas model to investigate CO_2 enhanced shale gas recovery and CO_2 storage capacity in shale formation. The structure of this paper is as follows. In first section, according to the multiple storage mode and multiple pore structure of shale gas reservoir with multiple fractured horizontal well (MFHW), the physical model of multi-continuum quadruple porosity shale gas reservoir was developed. In second section, On the basis of the physical model, the mathematical model was established, and which was solved by difference method (FDM) and quasi-Newton iterative method. In third section, the calculated result of this model was invalided by field data. In the last section, the sensitivity of serval main parameters was analyzed.

2. Physical model

According to previous study(He, Teng et al. 2016), the gas shale contains organic matters, organic pores, matrix pores and natural fractures. The gas stored in shale formation composed by three states gas, including dissolved gas in organic matters(Javadpour, Fisher et al. 2007,

Javadpour 2009). adsorbed gas on the surface of organics and clays and free gas stored in organic pores, matrix pores and natural fractures. Horizontal drilling and formation fracturing techniques are used to exploit shale gas, and serval main fractures and fracture networks are created after hydraulic fracturing. The region interconnected by moderate conductivity fracture networks is defined as stimulated reservoir volume (SRV), which is marked in blue in Fig. 1. The zone has not been influenced by fracturing is defined as un-stimulated reservoir volume (USRV), which is marked in black in Fig. 1.

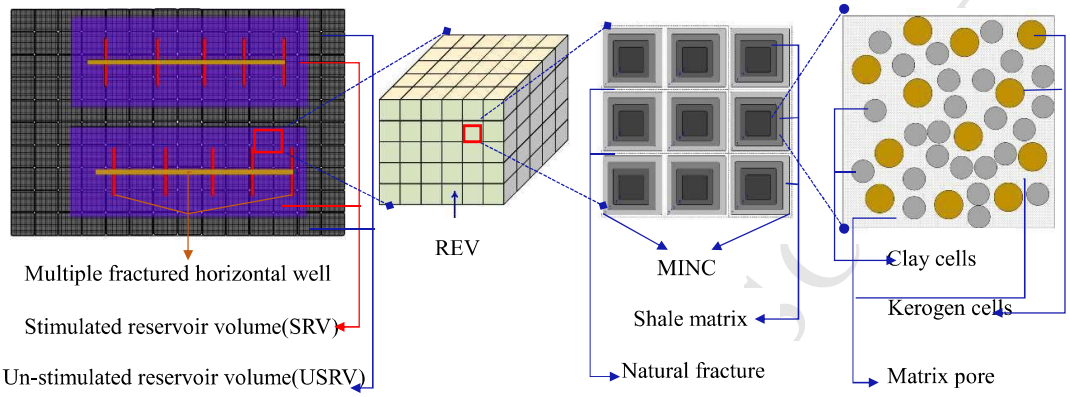

Fig. 1. Schematic diagram of a multi-continuum quadruple-porosity model for shale gas reservoirs.

As is shown in Fig. 1, a coupled multi-continuum quadruple porosity model is presented. The region marked in blue is the SRV, which can be simulated by quadruple-medium model, including natural fractures, matrix system, clay cells and kerogen cells. Because of the ultra-low permeability of shale matrix, the conventional dual-continuum model cannot be applicable to simulate the transfer flow between natural fracture and shale matrix any more, fortunately, multiple interacting continua (MINC) method can effectively be used to investigate the matrix-fracture transfer flow. Thus, a coupled multi-continuum quadruple porosity model is used to study the storage and transport mechanisms. In SRV, each representative elementary volume (REV) is divided into finite MINC elements, and each MINC element is divided into a series of nested sub-elements; each sub-element denotes different calculation element; the outer nested cell is natural fracture and the inner nested cell is matrix cells; clay cells and kerogen cells are contained in every nested cell. The region marked in black is the USRV, which can be simulated by triple porosity model, including matrix system, clay cells and kerogen cells.

The other assumptions of this proposed model are listed as follows:

(1) The dissolution of dissolved gas in organic matters obeys the Henry's law(Svrcek and Mehrotra 1982, Swami and Settari 2012), and the dissolved gas transport in organics can be driven by pressure difference diffusion, Knudsen diffusion and surface diffusion.

(2) The adsorption/desorption of each component gas on the surface of kerogen and clays follows Langmuir isothermal adsorption law, and different adsorption constant are considered for kerogen and clays, respectively.

(3) CO2 is mixed with CH_4 immediately, and the miscible time can be neglected.

(4) All hydraulic fractures fully penetrate the shale formation. Shale gas and carbon dioxide enter the horizontal wellbore only through hydraulic fractures from perforation location. Gas in matrix system and natural fracture system consists of compressed gas and adsorbed gas. The flow of gas in natural fracture system in SRV and the gas in matrix system in USRV obeys Darcy's law.

The effects of gravity and capillary pressure are neglected.

3. Mathematical model

3.1. Formulation of gas diffusion in kerogen cells

As discussed in model assumption, gas in kerogen cells consists of the free gas stored in kerogen pores, the adsorbed gas on the surface of organic pores and the dissolved gas in organic matters. Thus, the mass conservation equation of kerogen can be expressed as

$$\frac{\partial}{\partial t}\left[f_{\mathrm{k}}\phi_{\mathrm{k}}\rho_{\mathrm{gki}} + f_{\mathrm{k}}\left(1-\phi_{\mathrm{k}}\right)q^{\mathrm{e}}_{\mathrm{adk},i} + f_{\mathrm{k}}\left(1-\phi_{k}\right)q_{\mathrm{d},i}\right] - q_i^{\mathrm{m\text{-}k}} = -\nabla\cdot\left(\rho_{\mathrm{gki}}v_{\mathrm{gki}}\right), i=1,2 \quad (1)$$

In which, ρ_{gki} is the gas density of component i in kerogen cells, kg/m^3; v_{gki} denotes the gas flow velocity of component i in kerogen cells, m/s; ϕ_{k} is porosity of kerogen, fraction; $q^{e}_{\mathrm{adk},i}$ denotes the amount of component i remaining absorbed on the surface of kerogen, kg/m^3; $q_{\mathrm{d},i}$ denotes the amount of component i remaining dissolved in organic matters, kg/m^3; $q_i^{\mathrm{m\text{-}k}}$ denotes mass rate of kerogen-matrix transfer flow, kg/m^3; Subscript i refers to the gas species, with i=1 for methane and i=2 for carbon dioxide.

The migration of gas in kerogen cells can be driven by pressure difference diffusion, Knudsen diffusion and surface diffusion(Cao, Liu et al. 2017), and the total diffusivity related to pressure in kerogen system can be defined as

$$D_i = D_{\mathrm{p},i} + D_{\mathrm{kn},i} + D_{\mathrm{surf},i}, i=1,2 \quad (2)$$

where $D_{\mathrm{p},i}$ represents pressure driven diffusivity of component i, m^2/s; $D_{\mathrm{kn},i}$ denotes the effective Knudsen diffusivity of component i in kerogen cells, m^2/s; $D_{\mathrm{surf},i}$ is the surface diffusion coefficient of adsorbed gas in kerogen cells, m^2/s.

According to previous study(Cao, Liu et al. 2017), the apparent permeability for kerogen cells can be obtained by total diffusion coefficient, expressed as

$$k_{\mathrm{ka},i} = \frac{D_i\mu_g}{p_{\mathrm{k}}}, i=1,2 \quad (3)$$

In which, $k_{\mathrm{ka},i}$ denotes the apparent permeability for kerogen cells, μm^2; μ_{g} represents gas viscosity, mPa·s; p_{k} is the pressure in kerogens cells, MPa.

The motion equation can be derived from Darcy's law, given as

$$v_{\mathrm{gk}i} = -\frac{k_{\mathrm{ka},i}}{\mu_{\mathrm{g}}}\nabla p_{\mathrm{k}}, i=1,2 \quad (4)$$

Given the mole fraction of CH_4 in the bulk gas, the mole fraction of CO_2 is easily calculated since the two components satisfy the following equation, shown as

$$\omega_1 + \omega_2 = 1 \quad (5)$$

where ω_1 and ω_2 are the mole fraction of CH_4 and CO_2, respectively.

The mole fraction of component i can be expressed by the concentration of each component gas, given as

$$\omega_i = \frac{C_i}{C_1 + C_2}, i = 1,2 \tag{6}$$

where C_1 and C_2 are the molarity of CH_4 and CO_2, respectively.

According to the state equation, the partial pressure of each component gas can be obtained(Sun, Yao et al. 2013, Xu, Zeng et al. 2017), expressed as

$$p_i = p\omega_i = C_i Z_g RT, i = 1,2 \tag{7}$$

In which, Zg denotes the compressibility factors of mixture gas, the details is presented in previous studies(Jiang, Shao et al. 2014, Kim, Cho et al. 2017).

As is shown in Fig.1, the kerogen cells are embedded in matrix system, so, we need to simulate the transfer flow between matrix and kerogen cells. In this study, kerogen cells act as mass source in the multi-continuum quadruple porosity model. the transfer flow between matrix and kerogen can be simulated by the dual porosity model(Warren and Root 1963).The mass rate of kerogen-matrix transfer flow $q_i^{\text{m-k}}$, kg/m^3, can be expressed as

$$q_i^{\text{m-k}} = C_{\text{k},i} M_i \frac{\alpha k_{\text{ka},i}}{\mu_g} \left(p_{\text{m}} - p_{\text{k}} \right), i = 1,2 \tag{8}$$

$C_{\text{k},i}$ denotes molarity of component i in the kerogen, mol/m^3; M_i is molar mass of component i, fraction; According to previous studies(Sun, Yao et al. 2013, Jiang, Shao et al. 2014), competitive absorption between CO_2 and CH_4 exists in two gas components system, and the binary component Langmuir model can be used to estimate adsorption of each component, given as

$$q_{\text{adk},i} = \frac{\rho_{\text{k}} M_i}{V_{\text{std}}} \frac{V_{\text{Lk},i} p_i B_{ki}}{1 + \sum_j^2 p_j B_{\text{k}j}} = \frac{\rho_{\text{k}} M_i}{V_{\text{std}}} \frac{V_{\text{Lk},i} B_{ki} C_{\text{k},i} Z_g RT}{1 + \sum_{j=1}^2 C_{\text{k},j} B_{\text{k}j} Z_g RT}, i = 1,2 \tag{9}$$

In which, B_{ki} represents the inverse of Langmuir pressure of component i (B_{ki}=$p_{\text{L},i}$) , MPa^{-1}. V_{std} is the molar volume at standard condition, sm^3/mol; ρ_{k} denotes the density of kerogen, kg/m^3; $V_{\text{Lk},i}$ denotes the Langmuir volume constant of component i for kerogen system, sm^3/kg; p_1 and p_2 are the partial pressures of CH_4 and CO_2, respectively.

In fact, the concept of “excess adsorption” is usually used in adsorption measurements. Excess adsorption is the mass of gases stored in porous medium with adsorption in excess of the mass that would be stored if there were no adsorption at a given gas density (Edwards, Celia et al. 2015). Thus, the excess adsorption of component i can be formulated as

$$q_{\text{adk},i}^e = q_{\text{adk},i} \left(1 - \frac{\rho_{gi}}{\omega_i^a \rho_a} \right), i = 1,2 \tag{10}$$

where ρ_a denotes density of adsorption, kg/m^3, which is assumed to be constant and estimated from experimental excess adsorption data(Weniger, Kalkreuth et al. 2010); ω_i^a is adsorbed mass fraction of component i, given as

$$\omega_i^a = \frac{q_{\text{ad},i}}{q_{\text{ad},1} + q_{\text{ad},2}}, \quad i = 1,2 \tag{11}$$

Thus, the competitive excess absorption between CO_2 and CH_4 can be expressed as

$$q_{\mathrm{adk},i}^{e}=\frac{\rho_{\mathrm{k}}M_i}{V_{\mathrm{std}}}\frac{V_{\mathrm{Lk},i}B_{\mathrm{k}i}C_{\mathrm{k},i}Z_gRT}{1+\sum_{j=1}^{2}C_{\mathrm{k},j}B_{\mathrm{k}j}Z_gRT}\left[1-\frac{C_{\mathrm{k},i}M_i}{\rho_a}\left(1+\frac{M_jC_{\mathrm{k},j}V_{\mathrm{Lk},j}B_{\mathrm{k}j}}{M_iC_{\mathrm{k},i}V_{\mathrm{Lk},i}B_{\mathrm{k}i}}\right)\right],i,j=1,2\left(i\neq j\right) \quad (12)$$

The amount of component i remaining dissolved in organic matters in kerogen can be obtained by Henry's law(Swami and Settari 2012, He, Teng et al. 2016), expressed as

$$q_{\mathrm{d},i}=k_{\mathrm{H},i}p_{\mathrm{k},i}=k_{\mathrm{H},i}C_{\mathrm{k},i}Z_gRT,i=1,2 \quad (13)$$

In which, $k_{\mathrm{H},i}$ denotes solubility coefficient, $m^3/(Pa\cdot m^3)$.

Combining Eq. (6) ~ Eq. (9), the governing equation of component i in kerogen cells can be obtained, expressed as

$$\begin{aligned}&\frac{\partial}{\partial t}\left\{f_{\mathrm{k}}\left(1-\phi_{\mathrm{k}}\right)\frac{\rho_{\mathrm{k}}M_i}{V_{\mathrm{std}}}\frac{V_{\mathrm{Lk},i}B_{\mathrm{k}i}C_{\mathrm{k},i}Z_gRT}{1+\sum_{j=1}^{2}C_{\mathrm{k},j}B_{\mathrm{k}j}Z_gRT}\left[1-\frac{C_{\mathrm{k},i}M_i}{\rho_a}\left(+\frac{M_jC_{\mathrm{k},j}V_{\mathrm{Lk},j}B_{\mathrm{k}j}}{M_iC_{\mathrm{k},i}V_{\mathrm{Lk},i}B_{\mathrm{k}i}}\right)\right]\right\}\\&+\frac{\partial}{\partial t}\left[f_{\mathrm{k}}\phi_{\mathrm{k}}M_iC_{\mathrm{k},i}+f_{\mathrm{k}}\left(1-\phi_{\mathrm{k}}\right)k_{\mathrm{H},i}C_{\mathrm{k},i}Z_{\mathrm{g}}RT\right]\\&=\nabla\cdot\left(C_{\mathrm{k},i}M_i\frac{k_{\mathrm{ka},i}}{\mu_g}\nabla p_{\mathrm{k}}\right)+q_i^{\mathrm{m\text{-}k}},i,j=1,2\left(i\neq j\right)\end{aligned} \quad (14)$$

According to previous studies(Wilke 1950, Wu, Moridis et al. 2009), the viscosity values of mixture gas can be calculated by mole fraction and molar mass of each component gas, shown as

$$\mu_{\mathrm{g}}=\sum_{i=1}^{2}\frac{\mu_i}{1+\frac{1}{\omega_i}\sum_{j=1,j\neq i}^{2}\omega_j\varphi_{i,j}} \quad (15)$$

where $\varphi_{i,j}$ can be expressed as

$$\varphi_{i,j}=\frac{\left[1+\left(\mu_i/\mu_j\right)^{0.5}\left(M_j/M_i\right)^{0.25}\right]^2}{\left(4/\sqrt{2}\right)\left[1+\left(M_i/M_j\right)\right]^{0.5}} \quad (16)$$

3.2. Formulation of gas flow in matrix system

In USRV, gas in matrix system exists as adsorbed gas and free gas. The matrix pores are much larger than the organic pores, therefore, the surface diffusion of adsorbed gas on the surface of the clays can be ignored. Similar with the derivation in kerogen cell, the governing equation for gas flow in matrix system can be expressed as

$$\frac{\partial}{\partial t}\left[\left(1-f_{\mathrm{k}}\right)\phi_{\mathrm{m}}M_iC_{\mathrm{m},i}+\left(1-f_{\mathrm{k}}\right)\left(1-\phi_{\mathrm{m}}\right)q_{\mathrm{adc},i}^{\mathrm{e}}\right]=\nabla\cdot\left(\frac{k_{\mathrm{m}}}{\mu_{\mathrm{g}}}M_iC_{\mathrm{m},i}\nabla p_{\mathrm{m}}\right)+q_i^{\mathrm{m\text{-}k}},i=1,2 \quad (17)$$

where $C_{\mathrm{m},i}$ denotes molarity of component i in the matrix system, mol/m^3; ϕ_{m} is porosity of matrix system, fraction; p_{m} represents the gas pressure in matrix system, MPa; M_i is molar mass of component i; $q^{e}_{\mathrm{adc},i}$ denotes the amount of component i remaining absorbed on the surface of clays;

For clays in matrix system, the dual-component excess adsorption model can be used to

estimate the content of adsorption for each component gas, given as

$$q_{\mathrm{adc},i}^{e}=\frac{\rho_{\mathrm{c}}M_i}{V_{\mathrm{std}}}\frac{V_{\mathrm{Lc},i}B_{ci}C_{\mathrm{m},i}Z_gRT}{1+\sum_{j=1}^{2}C_{\mathrm{m},j}B_{\mathrm{c}j}Z_gRT}\left[1-\frac{C_{\mathrm{m},i}M_i}{\rho_a}\left(1+\frac{M_jC_{\mathrm{m},j}V_{\mathrm{Lc},j}B_{cj}}{M_iC_{\mathrm{m},i}V_{\mathrm{Lc},i}B_{\mathrm{c}i}}\right)\right],i,j=1,2\left(i\neq j\right) \quad (18)$$

Thus, the governing equation of component i in matrix in USRV can be obtained, expressed as

$$\begin{aligned}&\frac{\partial}{\partial t}\left\{\frac{\rho_{\mathrm{c}}M_i}{V_{\mathrm{std}}}\frac{V_{\mathrm{Lc},i}B_{ci}C_{\mathrm{m},i}Z_gRT}{1+\sum_{j=1}^{2}C_{\mathrm{m},j}B_{\mathrm{c}j}Z_gRT}\left[1-\frac{C_{\mathrm{m},i}M_i}{\rho_a}\left(1+\frac{M_jC_{\mathrm{m},j}V_{\mathrm{Lc},j}B_{cj}}{M_iC_{\mathrm{m},i}V_{\mathrm{Lc},i}B_{\mathrm{c}i}}\right)\right]\right\}\\&+\frac{\partial}{\partial t}\left[\left(1-f_{\mathrm{k}}\right)\phi_{\mathrm{m}}M_iC_{\mathrm{m},i}\right]-q_i^{\mathrm{m\text{-}k}}=\nabla\cdot\left(\frac{k_{\mathrm{m}}}{\mu_{\mathrm{g}}}M_iC_{\mathrm{m},i}\nabla\cdot p_{\mathrm{m}}\right),i=1,2\left(i\neq j\right)\end{aligned} \quad (19)$$

In SRV, matrix system was taken as source to apply liquid to natural fracture. As discussed in assumption above, the multiple interacting continua (MINC) method was used to simulate the transfer flow between matrix and natural fracture. As shown in Fig. 1, MINC element is divided into a series of nested sub-elements, and transfer flow exists between two adjacent sub-elements. The transfer flow rate can be calculated by following equation(Pruess and Narasimhan 1982, Pruess 2010), given as

$$q_{\mathrm{m},i}^{l,l+1}=\sigma A_{l,l+1}\left(\frac{k_{\mathrm{m}}}{\mu_{\mathrm{g}}}M_iC_{\mathrm{m},i,l}^{n+1}\frac{p_{\mathrm{m},i,l+1}^{n+1}-p_{\mathrm{m},i,l}^{n+1}}{d_{l,l+1}}\right) \quad (20)$$

$$q_{\mathrm{m},i}^{l,l-1}=\sigma A_{l,l-1}\left(\frac{k_{\mathrm{m}}}{\mu_{\mathrm{g}}}C_{\mathrm{m},i,l}^{n+1}M_i\frac{p_{\mathrm{m},i,l-1}^{n+1}-p_{\mathrm{m},i,l}^{n+1}}{d_{l,l-1}}\right) \quad (21)$$

In which, V_l is the volume of MINC sub-element l, m^3; $A_{l,l+1}$ donates the area of interface between element l and l+1, m^2; $\mathrm{d}_{l,l+1}$ donates the distance from element l to element l+1, m; the details can be found in previous study(Pruess and Narasimhan 1982, Pruess 2010, Jiang, Shao et al. 2014). σ is the number of elements contained in V_{m}, which is

$$\sigma=\frac{V_{\mathrm{m}}}{L^3} \quad (22)$$

where V_{m} is the volume of arbitrary a representative elementary volume (REV), m^3; L is the scale of MINC element, m.

Then the discretized governing equation of component i of sub-element l can be expressed as

$$\begin{aligned}&\frac{V_l}{\Delta t}\left\{\frac{\rho_{\mathrm{c}}M_i}{V_{\mathrm{std}}}\frac{V_{\mathrm{Lc},i}B_{ci}C_{\mathrm{m},i}Z_gRT}{1+\sum_{j=1}^{2}C_{\mathrm{m},j}B_{\mathrm{c}j}Z_gRT}\left[1-\frac{C_{\mathrm{m},i}M_i}{\rho_a}\left(1+\frac{M_jC_{\mathrm{m},j}V_{\mathrm{Lc},j}B_{cj}}{C_{\mathrm{m},i}M_iV_{\mathrm{Lc},i}B_{\mathrm{c}i}}\right)\right]\right\}_l^{n+1}\\&-\frac{V_l}{\Delta t}\left\{\frac{\rho_{\mathrm{c}}M_i}{V_{\mathrm{std}}}\frac{V_{\mathrm{Lc},i}B_{ci}C_{\mathrm{m},i}Z_gRT}{1+\sum_{j=1}^{2}C_{\mathrm{m},j}B_{\mathrm{c}j}Z_gRT}\left[1-\frac{C_{\mathrm{m},i}M_i}{\rho_a}\left(1+\frac{M_jC_{\mathrm{m},j}V_{\mathrm{Lc},j}B_{cj}}{C_{\mathrm{m},i}M_iV_{\mathrm{Lc},i}B_{\mathrm{c}i}}\right)\right]\right\}_l^{n}\\&+\frac{V_l}{\Delta t}\left[\left(1-f_{\mathrm{k}}\right)\phi_{\mathrm{m}}M_iC_{\mathrm{m},i}\right]_l^{n+1}-\frac{V_l}{\Delta t}\left[\left(1-f_{\mathrm{k}}\right)\phi_{\mathrm{m}}M_iC_{\mathrm{m},i}\right]_l^{n}\\&=q_{\mathrm{m},i}^{l,l+1}+q_{\mathrm{m},i}^{l,l-1},i=1,2\left(i\neq j\right)\end{aligned} \quad (23)$$

3.3. Formulation of gas flow in natural fractures

The permeability of natural fractures is much larger than the matrix system and kerogen system, the main migration mechanism in natural fractures is viscous flow, so the diffusion can be neglected. Then, the governing equation for the dual component mixture gas flow in natural fractures can be obtained, expressed as

$$\frac{\partial}{\partial t}\left(\phi_{\mathrm{f}} C_{\mathrm{f},i} M_i\right) = \nabla \cdot \left(\frac{k_{\mathrm{f}}}{\mu_g} C_{\mathrm{f},i} M_i \nabla p_{\mathrm{f}}\right) + q_i^{\mathrm{conn}}, i = 1,2 \tag{24}$$

where q_i^{conn} denotes gas flow rate between matrix and natural fractures, m^3/s, which can be calculated by Eq. (20) because natural fractures are located at the outer of nested cell of MINC element.

According to previous study(Zhu, Yao et al. 2016), permeability sensitivity should be considered in natural fracture because they are un-propped, and the natural fracture permeability can be expressed as a function of initial fracture permeability k_{f}^0, the permeability modulus of natural fracture γ and the pressure in natural fracture p_{h}, which is

$$k_{\mathrm{f}} = k_{\mathrm{f}}^0 e^{-\gamma\left(p_{\mathrm{f}} - p_0\right)} \tag{25}$$

In which, k_{f}^0 is the absolutely permeability, μm^2; b_{k} is the Klingenberg factor, MPa.

Then the governing equation of component i in natural fractures can be presented as Eq. (26).

$$\frac{\partial}{\partial t}\left(\phi_{\mathrm{f}} M_i C_{\mathrm{f},i}\right) = \nabla \cdot \left[\frac{M_i k_{\mathrm{f}}^0}{\mu_{\mathrm{g}}} e^{-\gamma\left(p_{\mathrm{f}} - p_0\right)} C_{\mathrm{f},i} \nabla p_{\mathrm{f}}\right] + q_i^{\mathrm{conn}}, i = 1,2 \tag{26}$$

3.4. Formulation of gas flow in hydraulic fracture

The hydraulic fracture created by fracturing, enlarged the contact area of horizontal well and shale formation, is the ideal gas channel around horizontal well. Combing gas motion equation, gas state equation and continuity equation, the governing equation of hydraulic fractures can be derived, presented as

$$\frac{\partial}{\partial t}\left(\phi_{\mathrm{h}} C_{\mathrm{h},i} M_i\right) = \nabla \cdot \left(\frac{k_{\mathrm{h}}}{\mu_{\mathrm{g}}} C_{\mathrm{h},i} M_i \nabla p_{\mathrm{h}}\right), i = 1,2 \tag{27}$$

where $C_{\mathrm{h},i}$ denotes molarity of component i in hydraulic fracture, mol/m^3; ϕ_{h} is porosity of hydraulic fracture, fraction; p_{h} denotes the gas pressure in hydraulic fracture, MPa; k_{h} is permeability of hydraulic fracture, μm^2;

The Knudsen number for the gas flow in hydraulic fractures is in the high Knudsen number regime(Xu, Zeng et al. 2017), so the slip flow for gas in hydraulic fractures should be considered, which also is called Klingenberg effect, given as

$$k_{\mathrm{h}} = k_{\infty}\left(1 + \frac{b_{\mathrm{k}}}{p_{\mathrm{h}}}\right) \tag{28}$$

where p_0 is the initial pressure of shale reservoir, MPa. Then the governing equation of hydraulic fracture can be presented as

$$\frac{\partial}{\partial t}\left(\phi_{\mathrm{h}} M_i C_{\mathrm{h},i}\right)=\nabla\cdot\left[\frac{M_i k_{\infty}}{\mu_{\mathrm{g}}}\left(1+\frac{b_{\mathrm{k}}}{p_{\mathrm{h}}}\right)C_{\mathrm{h},i}\nabla p_{\mathrm{h}}\right], i=1,2 \tag{29}$$

3.5. Numerical solution

Finite difference method (FDM) was used to solve this fully coupled multi-continuum quadruple porosity binary component gas model. The governing equations of the kerogen system, the matrix system in the USRV, the natural fractures and the hydraulic fractures were discretized by fully implicit scheme. Time discretization is carried out using forward difference scheme.

The embedded discrete fracture model (EDFM), established by(Li and Lee (2008), Moinfar, Varavei et al. (2014)), was used to simulate the flow of hydraulic fractures and the transfer flow between natural fractures and hydraulic factures, and the transfer flow rate can be expressed by

$$q_i^{\text{h-f}}=\frac{k_{\text{h-f}}A_{\text{h-f}}M_i C_{i,\text{h-f}}^{n+1}}{\mu_g}\frac{p_{i,\text{h}}^{n+1}-p_{i,\text{f}}^{n+1}}{d_{\text{h-f}}} \tag{30}$$

where $k_{\text{h-f}}$ denotes the transfer flow permeability between natural fracture and hydraulic facture, μm^2; $A_{\text{h-f}}$ is the transfer area, m^2; $d_{\text{h-f}}$ is the transfer distance, m. $C_{i,\text{h-f}}^{n+1}$ denotes the molarity of component i transfer flow between hydraulic fractures and natural fractures. The more details can be found in previous studies(Li and Lee 2008, Moinfar, Varavei et al. 2014).

According to the method proposed by Moinfar, Varavei et al. (2014), the flow rate of component i between hydraulic fractures and horizontal well can be expressed as

$$q_{\text{h-w}}=WI\_h\cdot M_i C_{i,\text{h-w}}^{n+1}\left(p_{\text{h}}^{n+1}-p_{\text{w}}^{n+1}\right) \tag{31}$$

where $C_{i,\text{h-w}}^{n+1}$ denotes the molarity of component i transfer flow between hydraulic fractures and horizontal wellbore, mol/m^3; WI_h is the well index, expressed as

$$WI\_h=\frac{2\pi w_{\text{h}}}{\ln\left(0.14\sqrt{h^2+\Delta l_{\text{h}}{}^2}\right)+S_{\text{h}}} \tag{32}$$

where ω_{h} is the width of hydraulic fracture, m; S_{h} is the skin factor of hydraulic fracture around horizontal well, dimensionless; h is the gas reservoir thickness, m; Δl_{h} is the fracture length bounded in the hydraulic fracture element, m;

The finite difference method was used to solved this model, the governing equations of each media were discretized into differential form. The full implicit central difference in space and forward difference in time term were employed to discretize the equations. Then, these differential equations of each media were coupled, and the embedded discrete fracture model (EDFM) was used to simulate the flow between hydraulic fracture and natural fracture in SRV. The model proposed in this paper is fully coupled and strongly nonlinear due to the multiple flow mechanisms of binary component gas in shale formation. Due to the strongly nonlinear of the numerical equations for this model, conventional linear numerical method is helpless. In order to solve this model successfully, the quasi-Newton iterative method was used to solve the solution of numerical equations, the numerical solution is implemented in MATLAB.

As all we known, the numerical convergence and stability are quite important for numerical simulations. The governing equations are discretized by implicit method, which is unconditionally

stable(Jiang, Shao et al. 2014). Moreover, the Jacobi matrix of the nonlinear differential equations derived above paragraph is symmetric positive definite, so the quasi-Newton iterative method is convergent in second order.

4. Discussion

The basic parameters for injection CO_2 into shale gas reservoir was presented in table 1, Based on which, a shale gas mining simulation with carbon dioxide injection was performed to investigate the injectivity of CO_2 in shale gas reservoirs and CO_2 enhanced natural gas recovery. The total production period is 6000 days, and CO_2 was injected in shale formation through well-2 after 2000 days. Then, the pressure distribution and mole fraction distribution of mixture gas can be solved by this proposed model, which were shown in Fig. 2 and Fig. 3, respectively.

Table 1 Basic reservoir parameters for the calculation based on this proposed model.

Parameters	Value	Parameters	Value
Initial pressure, p_i (MPa)	12	Herry's constant of CH_4, k_{H1} (m^3/Pa/m^3)	5.9×10^{-7}
Wellbore pressure, p_{wf} (MPa)	3.6	Herry's constant of CO_2, k_{H2} (m^3/Pa/m^3)	2.5×10^{-6}
Injection pressure, p_{inj} (MPa)	8.6	Sensitivity coefficient, γ, (MPa^{-1})	1×10^{-10}
Reservoir temperature, T(K)	353	Slipping coefficient, b_k, (MPa)	7.6×10^{5}
Fracture skin factor, S_f	-1	Hydraulic fracture number, N_f	7
Production period, time (day)	6000	Hydraulic fracture spacing, (m)	80
Porosity of matrix, ϕ_m	0.1	CH_4 Langmuir volume in kerogen, V_{L1k}(m^3/kg)	0.0023
Porosity of kerogen, ϕ_k	0.3	CO_2 Langmuir volume in kerogen, V_{L2k}(m^3/kg)	0.0086
Porosity of hydraulic fracture, ϕ_h	0.5	CH_4 Langmuir volume in matrix, V_{L1c}(m^3/kg)	0.0015
Volumetric fraction of kerogen, f_k	0.3	CO_2 Langmuir volume in matrix, V_{L2c}(m^3/kg)	0.0053
Density of rock, ρ_{sc}(kg/m^3)	2600	CH_4 Langmuir pressure in kerogen, P_{L1k}(MPa)	6.54
Density of kerogen k_h(kg/m^3)	1500	CO_2 Langmuir pressure in kerogen, P_{L2k}(MPa)	2.05
Diffusivity of CH_4, D_1(m^2/s)	2.5×10^{-16}	CH_4 Langmuir pressure in matrix, P_{L1c}(MPa)	7.86
Diffusivity of CO_2, D_2 (m^2/s)	4.5×10^{-16}	CO_2 Langmuir pressure in matrix, P_{L2c}(MPa)	1.52
Gas viscosity of CH_4, μ_{g1}(Pa·s)	1.61×10^{-5}	Matrix permeability, k_m(μm^2)	1×10^{-5}
Gas viscosity of CO_2, μ_{g2}(Pa·s)	3.24×10^{-5}	Natural fracture permeability, k_m(μm^2)	1×10^{-3}
Reservoir thickness, h (m)	50	Hydraulic-fracture permeability k_h(μm^2)	1×10^{3}

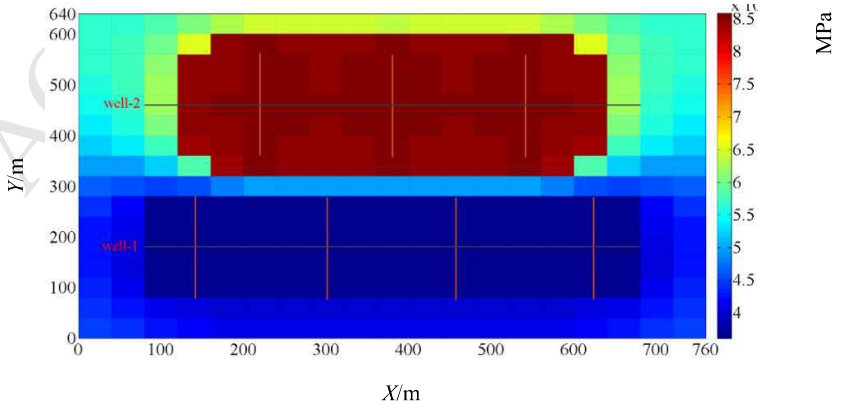

Fig. 2. Pressure distribution of gas reservoir on 2200th day.

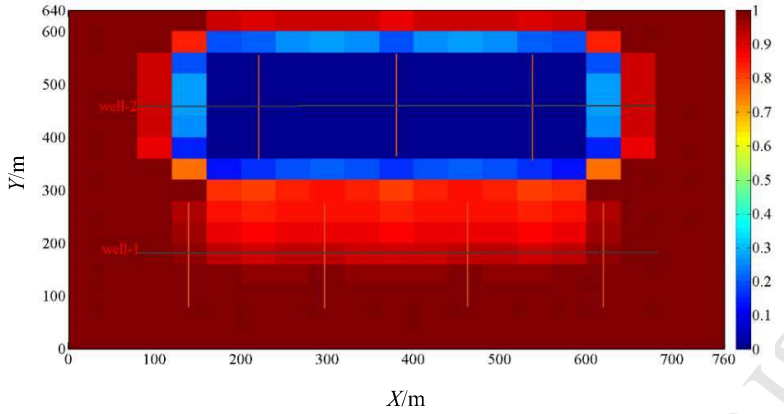

Fig. 3. Mole fraction distribution of gas reservoir on 2200th day.

Fig. 2 and Fig. 3 shows the pressure distribution and mole fraction distribution for outer nested-cell of natural fracture continuum in SRV and matrix system in USRV on 2200th days. The pressure in SRV around well-2 is higher than that around well-1, which means that injectivity of CO_2 can make shale formation re-pressurized, and SRV is beneficial to CO_2 injection and CO_2 enhanced natural gas recovery. The CH_4 mole fraction distribution can indicate the location of CO_2 injected from well-2, a smaller CH_4 mole fraction means that the more CO_2 was stored here. As is shown in Fig. 3, the CH_4 mole fraction in SRV around well-2 is close to zero, and the CH_4 mole fraction in the zone between well-1 and well-2 is also lower than that in remaining zone around well-1, the reason is that the SRV has high conductivity due to the interconnected natural fracture network, so CO_2 can migrate through the SRV easily.

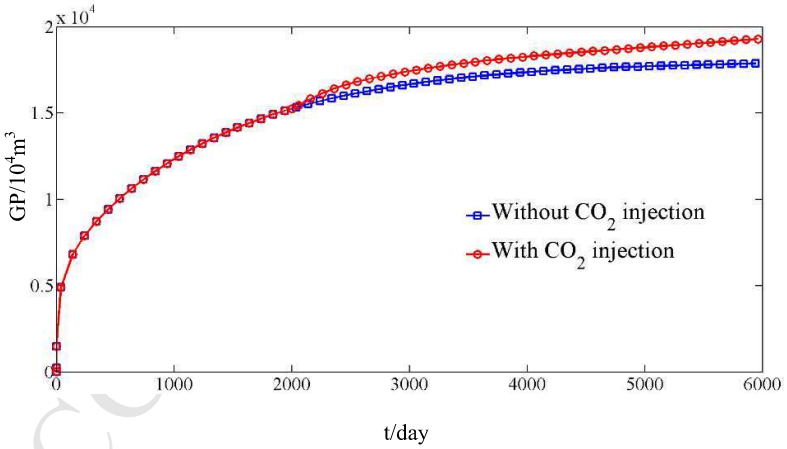

Fig. 4. Effect of CO_2 injection on CH_4 cumulative production curves.

Fig. 4 shows effect of CO_2 injection on CH_4 cumulative production curves, the slope of CH_4 cumulative production curve increased shortly after carbon dioxide injection. CO_2 from injection well drives CH_4 from stagnant zone into production well, so that CH_4 cumulative production increases faster. As discussed in assumption, CO_2 is mixed with CH_4 immediately, moreover, the distance between the SRV around injection and that around production well is very short (as shown in Fig. 3), so that CO_2 injection can soon influence the CH_4 cumulative production. As is shown in Fig. 4, injecting CO_2 into shale gas reservoir can significantly increase natural gas cumulative production. The reason is that CO_2 injection improves the production rate of CH_4 by reservoir re-pressurization and CH_4 replacement by CO_2. Therefore, injectivity of CO_2 into shale

gas reservoir is feasible technology to sequestrate CO_2 and enhanced CH_4 recovery in shale gas reservoir.

4.1. Validation

Due to few samples of CO_2 injection into shale gas reservoir are implemented successfully around the world, it is difficult to find field data to verify this proposed model. In order to validate the reliability and practicality of the model in this paper, published shale gas reservoir production data of a well from (He, Teng et al. (2016)) was used. This shale gas reservoir with fractured horizontal well have long production period, so this proposed model is appropriate to match the production history of this reservoir. Combining parameter search method, this proposed model was used to obtain fitting parameters along the given reservoir parameters and production history data. We first adjust the physical model as a boxed shale gas reservoir with a fractured horizontal well. The 12 hydraulic fractures are symmetrical and vertical to the horizontal well. The more detailed input parameters for matching production history of well-3 is listed in Table 2.

Table 2 Input parameters for matching production history of well-3.

Parameters	Value	Parameters	Value
Initial pressure, p_i (MPa)	20.34	Hydraulic-fracture half length, x_f (m)	75
Wellbore pressure, p_{wf}(MPa)	3.45	Length of horizontal well: L_H (m)	1006
Reservoir temperature, T(K)	335	Hydraulic fracture number, N_f	12
Thickness of formation: h (m)	46	Gas viscosity, μ_g(μm^2)	0.022
Porosity of fracture, ϕ_f	0.0045	Fracture skin factor, S_f	0.2
Grid size, (m)	50×50	Sensitivity coefficient, γ, (MPa^{-1})	1×10^{-9}
Slipping coefficient, b_k, (MPa)	6×10^5	Production period, time (day)	800

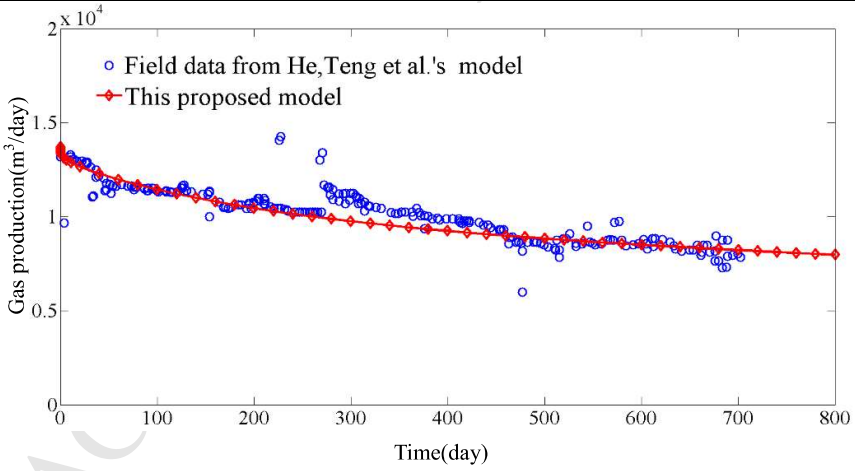

Fig.5. Comparison of the field data to this proposed model.

With the given parameters fixed, when we changed the fitting parameters, the shale gas production curve changed as well. So, we performed amount of simulation test to find the most appropriate parameters, with which the result of this model matches the production history best. As is shown in Fig. 5, the line data marked in red is the results derived from this proposed model, and the point data marked in blue represents field data from well-3. The matching results calculated by this proposed model is listed in Table 3, which is close to the result derived by (He, Teng et al. (2016)). It indicates that this proposed model can match well with the production history, moreover, this model can be used to predict the production of the fractured horizontal well

in this reservoir. Therefore, our model is reasonable and practical.

Table 3 Matching results calculated by this proposed model.

Parameters	Value
Natural fracture permeability, k_f (μm^2)	0.001
Solubility coefficient, k_{H1} ($m^3/Pa/m^3$)	1.9×10^{-6}
CH_4 diffusion coefficient, D_1 (m^2/s)	5×10^{-17}
Hydraulic fracture permeability k_h (μm^2)	800
Matrix permeability, k_m (μm^2)	9×10^{-5}

4.2. Sensitivity analysis

4.2.1. Adsorption parameters

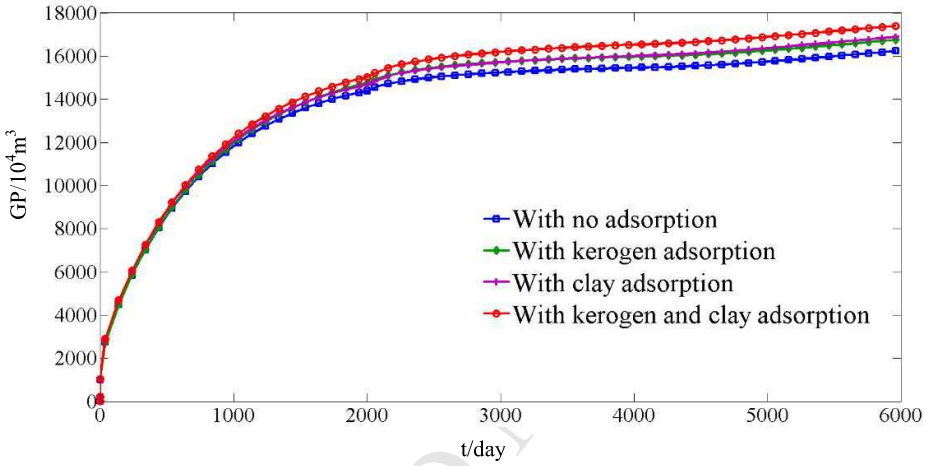

Fig. 6. The effect of adsorption on CH_4 cumulative production curves.

Fig. 6 and Fig. 7 show the effect of adsorption on CH_4 cumulative production curves and CO_2 storage capacity curves, respectively. When this model come to four different adsorption cases, including the model with no adsorption, with clay adsorption only, with kerogen adsorption only and with both two adsorptions. The CH_4 cumulative production and CO_2 storage capacity increase as the model varies from case 1 to case 4. The reason is that the stronger the adsorption ability of shale formation, the more adsorbed natural gas was exploited during producing, and the more CO_2 adsorbed on the surface of porous media during competitive absorption between CO_2 and CH_4.

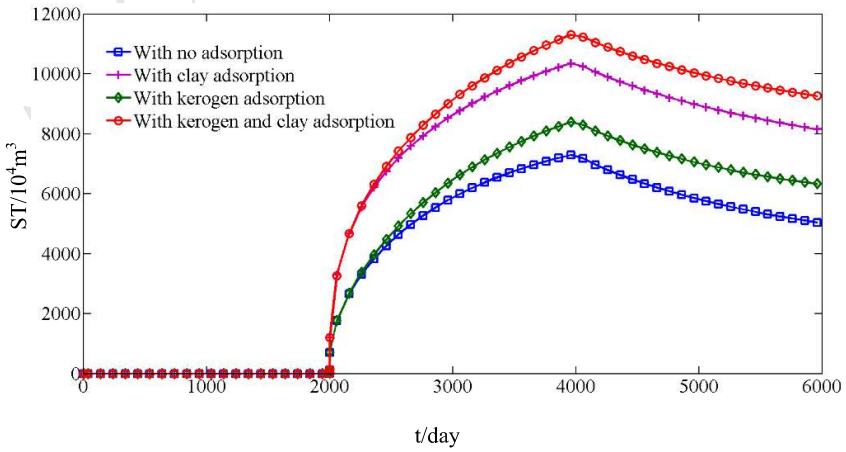

Fig. 7. The effect of adsorption on CO_2 storage capacity.

As is shown in Fig 7, CO_2 storage capacity is increased about 60% when the kerogen and clay adsorption was considered in this proposed model. The reasons are as follows. After carbon dioxide is injected into shale gas reservoirs, some of CO_2 is stored in natural fracture and matrix pore, some of CO_2 is adsorbed on the surface of kerogen and clay, and the other part of CO_2 is dissolved into organic matter. At the same time, the production well is mining, when CO_2 arrives the production wellbore, it will be exploited. So, most of the CO_2 stored in natural fracture and matrix pores will be mined out, while the adsorption CO_2 and dissolved CO_2 are difficult to be exploited, so they are sequestrated in shale formation forever. Therefore, the CO_2 storage capacity mainly depends on the adsorption and dissolution of shale formation for CO_2.

4.2.2. Dissolution parameters

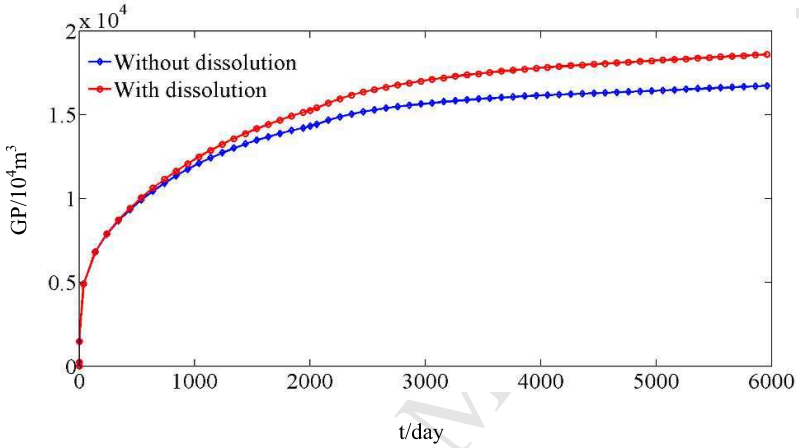

Fig. 8. The effect of dissolution on CH_4 cumulative production curves.

Fig. 8 and Fig. 9 show the effect of dissolution on CH_4 cumulative production curves and CO_2 storage capacity curves, respectively. The CH_4 cumulative production and CO_2 storage capacity increase significantly when considering the gas dissolved in organics. This is because both CH_4 and CO_2 can be dissolved in organic matters, dissolved methane diffuses into matrix pores during depressurization producing and improve the final natural gas production; Carbon dioxide will be dissolved in organics during injection process, which can increase the CO_2 storage capacity greatly. Therefore, the dissolution of CH_4/CO_2 for organic matters so important for CO_2 storage and CO_2 enhanced shale gas recovery that it cannot be neglected. Moreover, the dissolution of CH_4/CO_2 can effectively increase the CO_2 storage capacity and CH_4 final cumulative production.

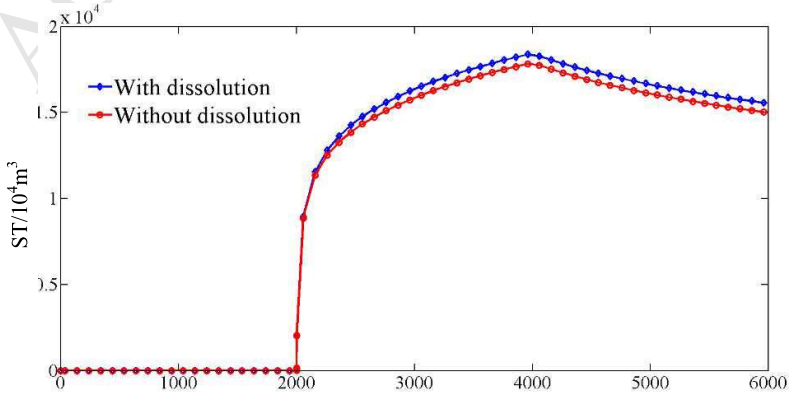

t/day

Fig. 9. The effect of dissolution on CO_2 storage capacity.

4.2.3. Production pressure

Fig. 10 and Fig. 11 show the effect of production pressure of well-1 p_{wfl} on CH_4 cumulative production curves and CO_2 storage capacity curves, respectively. It is very obvious that p_{wfl} has significant impact, with all other parameters kept fixed, on CH_4 cumulative production and CO_2 storage capacity. The larger the value of p_{wfl} is, the less shale gas will be obtained, and the less carbon dioxide will be injected in shale formation. The main reason is that a larger value of p_{wfl} leads to less energy loss in shale gas reservoir, which means that more CH_4 will be still stored, and less CO_2 can be injected in shale formation. However, the lower pressure of production well p_{wfl} is, the more CO_2 will be exploited, so that less CO_2 will be sequestrated in shale formation, which is shown in Fig. 11.

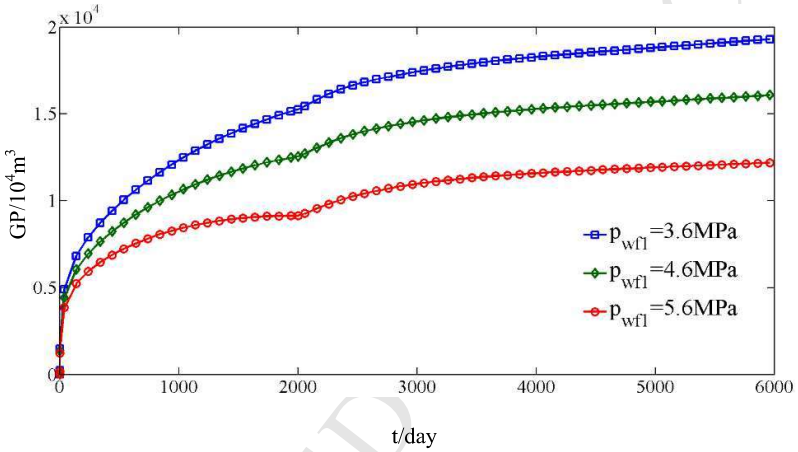

Fig. 10. The effect of production pressure on CH_4 cumulative production curves.

The CO_2 injection has been performed from 2000th day to 4000th day, after 4000th day, the CO_2 injection was stopped, while the production well continued to produce and part of CO_2 was mined out. So, the amount of CO_2 storage increases from 2000th day to 4000th day, then it decreases after 4000th day, which is shown in Fig. 11.

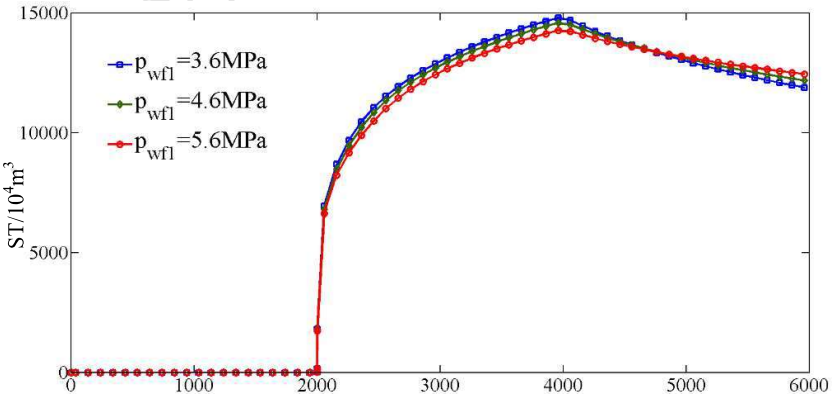

Fig. 11. The effect of production pressure on CO_2 storage capacity.

Fig. 12 shows the effect of production pressure of well-1 p_{wfl} on CO_2 cumulative production

curves. The higher the production pressure is, the lower CO_2 cumulative production curve is. This is because that the higher production pressure leads to less energy loss, so the less CO_2 can be exploited from the production well.

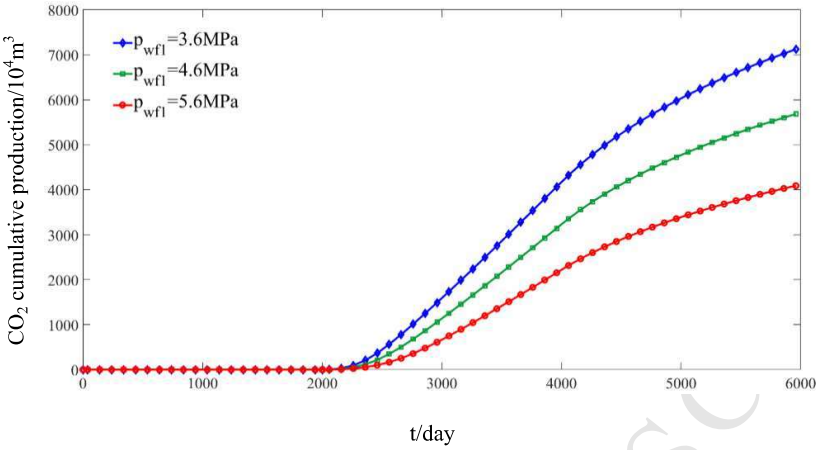

Fig. 12. The effect of production pressure on CO_2 cumulative production curve.

4.2.4. Injection pressure

Fig. 13 shows the effect of injection pressure of well-2 p_{wf2} on CO_2 storage capacity curves. p_{wf2} has significant effect on CO_2 storage capacity curves, and the larger the value of p_{wf2} is, the more carbon dioxide is sequestrated in shale formation. The reason is that a larger value of p_{wf2} means that more CO_2 can be injected and stored in shale formation, so the CO_2 storage capacity curves are higher.

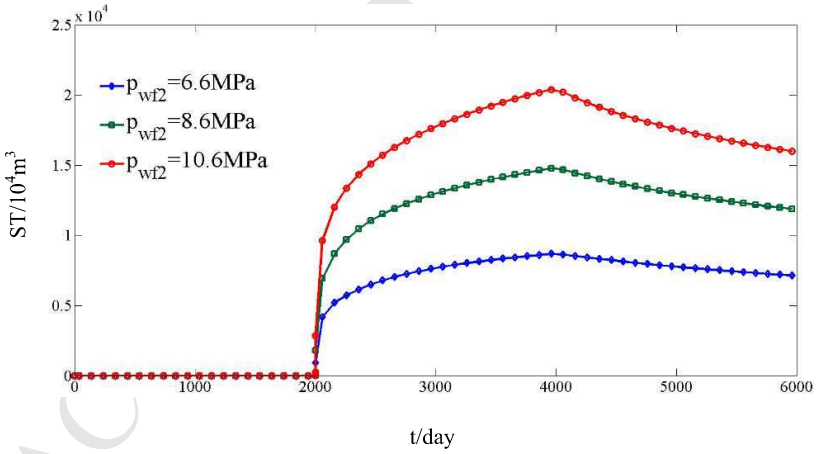

Fig. 13. The effect of injection pressure on CO_2 storage capacity.

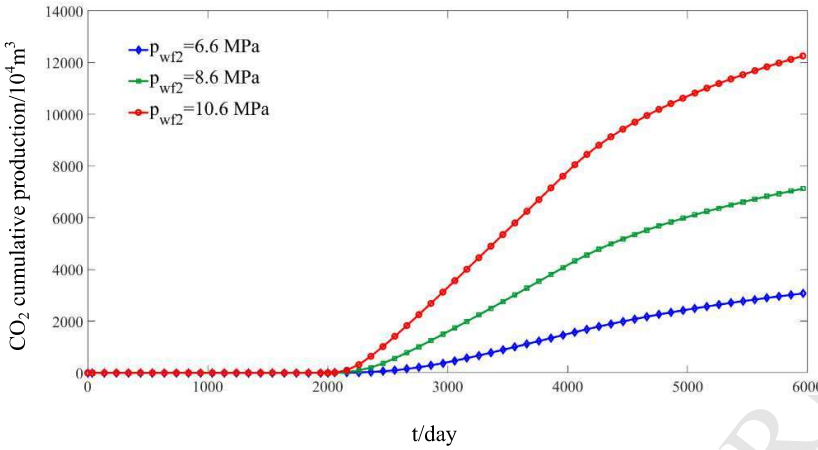

Fig. 14. The effect of injection pressure on CO_2 cumulative production curves.

Fig. 14 shows the effect of injection pressure of well-2 p_{wf2} on CO_2 cumulative production curves. The larger the value of injection pressure is, the CO_2 cumulative production is higher. The reason is that the higher injection pressure enforced the CO_2 flow, so the more CO_2 can be exploited from the production well.

4.2.5. Volumetric fraction of kerogen f_k

Fig. 15 shows the effect of volumetric fraction of kerogen f_k on CH_4 cumulative production curves. The larger the value of f_k is, the more natural gas is obtained. The reason is that a larger volumetric fraction of kerogen indicates a higher total organic-carbon content, which means that more natural gas in dissolved state come out from organics, and more adsorbed gas was stored in kerogen cells. Thus, a shale gas reservoir with larger volumetric fraction of kerogen have more natural gas stored in shale formation.

Fig. 16 shows the effect of volumetric fraction of kerogen f_k on CO_2 storage capacity curves. The larger the value of f_k is, the less carbon dioxide is stored in shale formation. The reason is that a larger volumetric fraction of kerogen means that the volumetric fraction of inorganic matrix is small, which is the main storage space of CO_2, then less CO_2 can be sequestrated in shale formation.

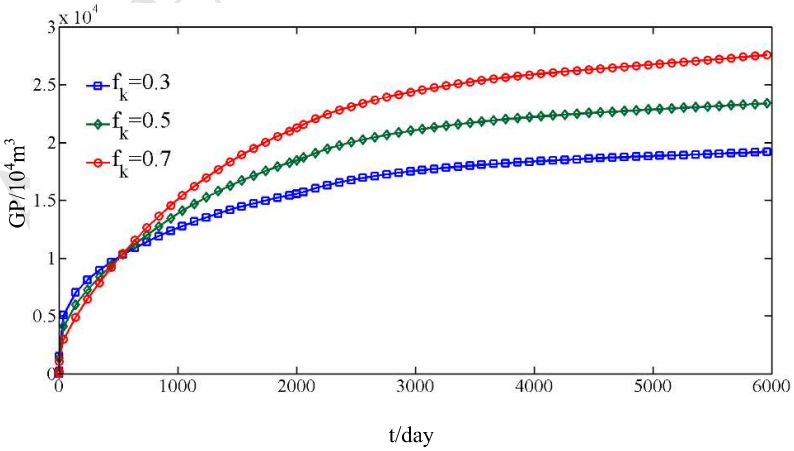

Fig. 15. The effect of volumetric fraction of kerogen f_k on CH_4 cumulative production curves.

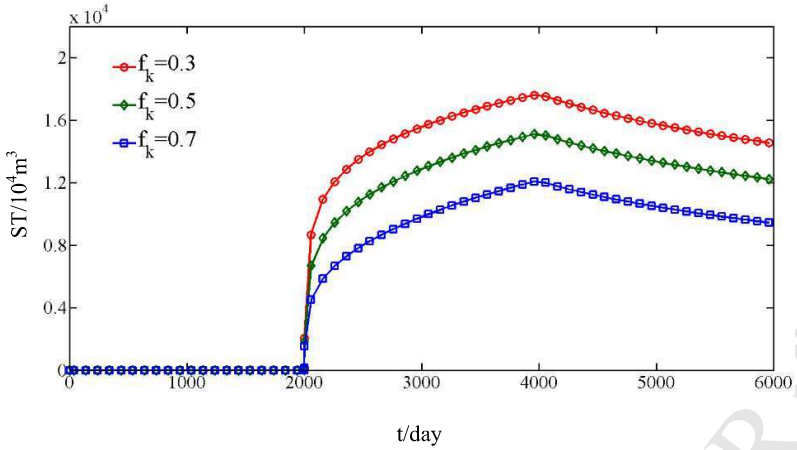

Fig. 16. The effect of volumetric fraction of kerogen f_k on CO_2 storage capacity.

4.3. Injection opportunity

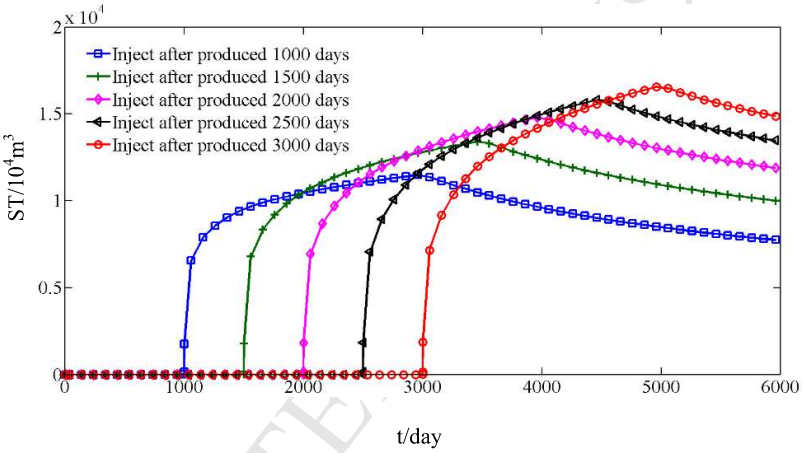

Fig. 17. The effect of injection opportunity on CO_2 storage capacity.

Fig. 17 shows the effect of CO_2 injection opportunity on CO_2 storage capacity curves. The later the injection starting time is, setting injection duration fixed to 2000 days, the more carbon dioxide is sequestrated in shale formation. This is because that the later injection starting time results in lower energy of shale formation around the p_{wf2}, which increases the CO_2 storage capacity greatly. As is shown in Fig. 17, when the injection starting time increases from 1000th day to 3000th day, the increment of CO_2 storage capacity decreases clearly. The reason is that CO_2 storage capacity is determined by many factors, such as adsorption and the content of organics, which limits CO_2 storage capacity greatly as the energy of shale formation decreases.

4.4. Injection strategy

Fig. 18 show the CH_4 cumulative production curves of three cases with different injection strategies. We fixed the total period as 7000 days, then, the CO_2 huff-n-puff patterns are shown as follows. There is no injection in Case 1, which means that the wells have produced for 7000 days, denoted as (P_7000). One huff-n-puff is involved in Case 2, then, Case 2 includes production period, soak period and injection period, can be expressed as (P_2000+I_1500+S_1500+P_2000). Case 3 was denoted as (P_1000+I_500+S_500+P_1000+I_1000+S_1000+P_2000).

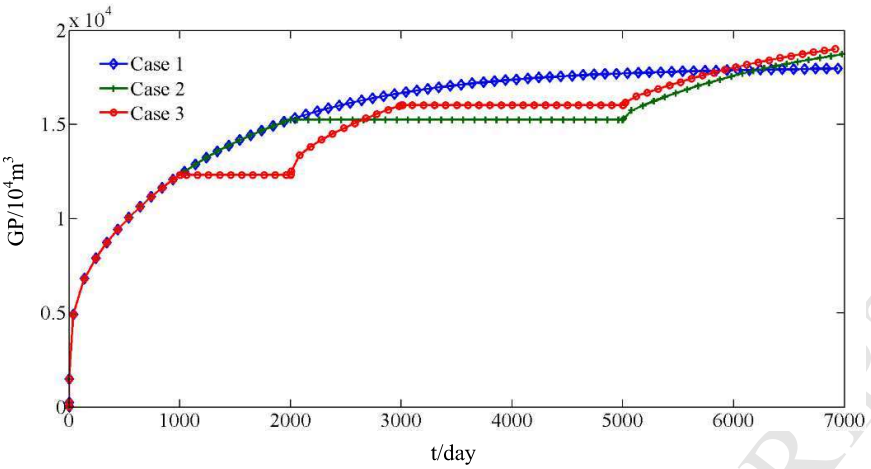

Fig. 18. The CH_4 cumulative production curves of three injection strategies.

As is shown in Fig. 18, it is clear that the ultimate cumulative CH_4 production of Case 1 is the lowest among these cases. Although the total injection period, total soak period and total production period are the same in Case 2 and Case 3, the Case 3 has higher ultimate cumulative CH_4 production. This is because that more huff-n-puff are involved in Case 3, and repeatedly implementing CO_2 huff-n-puff can improve reservoir re-pressurization and CH_4 replacement by CO_2.

5. Conclusions

This paper developed a multi-continuum quadruple porosity binary component model to investigate CO_2 storage and CO_2 enhanced shale gas recovery. According to the results presented above, the following conclusions are obtained:

(1) The mathematical model for CO_2 geologic sequestration in shale gas reservoir is established with multiple flow mechanisms including dissolution, adsorption/desorption, viscous flow, diffusion, slip flow and stress sensitivity of hydraulic fractures. Moreover, this proposed model is coupled by quadruple media, including natural fractures, matrix system, clay cells and kerogen cells.

(2) The transfer flow between matrix system and natural fractures is simulated by modified multiple interacting continua (MINC) method, and embedded discreate fracture model (EDFM) is introduced to simulate the gas flow in hydraulic fractures and the transfer flow between hydraulic fractures and natural fractures. This model was solved by finite difference method and quasi-Newton iterative method. The theoretical stability and convergence of solving method have been presented.

(3) This model can match well with the production history of the fractured horizontal well of a shale gas reservoir, which means this proposed is reliable and practicable.

(4) Sensitivity analysis of serval uncertain parameters was given above, which offers meaningful theoretical reference on estimating carbon dioxide storage capacity and CO_2 enhanced shale gas recovery.

(5) Injection opportunity and injection strategy for CO_2 sequestrated in shale formation has been analyzed, which is helpful to determine the better CO_2 injection strategy for CO_2 enhanced shale gas recovery.

Acknowledgement

This work was supported by the Changjiang Scholars and Innovative Research Team Development Program "Theory and technology in complex reservoir development and EOR theory" (IRT1294) and the National High Technology Research and Development Program (863 Program) "Key technologies in deep water oil fields intelligent completion" (2013AA09A215).

Nomenclature

ϕ_f,	porosity of natural fracture system, dimensionless;
ϕ_m,	porosity of matrix system, dimensionless;
ϕ_k,	porosity of kerogen system, dimensionless;
ϕ_h,	porosity of hydraulic fracture system, dimensionless;
p_{sc}	pressure under the ground condition, Pa;
p_i	pressure under the initial reservoir condition, Pa;
$p_{L,i}$	Langmuir pressure of component i, i=1, 2, Pa;
$V_{L,i}$	Langmuir volume of component i, i=1, 2, Pa;
α	shape factor of shale matrix element, m^{-2};
$k_{m,}$	shale matrix permeability, m^2;
k_{fi}	natural fracture absolute permeability, m^2;
k_h	hydraulic fracture permeability at initial condition, m^2;
$k_{H,i}$	Solubility coefficient, $m^3/(Pa \cdot m^3)$;
$D_{p,i}$	pressure driven diffusivity of component i, m^2/s;
$D_{kn,i}$	Knudsen diffusivity of component i in kerogen cells, m^2/s;
$D_{surf,i}$	surface diffusion coefficient of adsorbed gas in kerogen cells, m^2/s;
ω_1 ω_2	mole fraction of CH_4 and CO_2, fraction, respectively;
μ_g	shale gas viscosity, Pa·s;
Z_g	gas compressibility factor;
Q_1	production rate of CH_4, m^3/s;
Q_2	production rate of CO_2, m^3/s;
$q_{ad,i}$	The amount of component i remaining absorbed on the surface of kerogen, kg/m^3;
$q_{d,i}$	The amount of component i remaining dissolved in organic matters, kg/m^3;
$q_i^{m\text{-}k}$	The mass rate of kerogen-matrix transfer flow, kg/m^3;
GP	cumulative production of CH_4, m^3;
ST	cumulative storage capacity of CO_2, m^3;
N_f	quantity of hydraulic fracture;
x, y	x- and y-coordinates, m;
t	time, s;
M_1 M_2	molar mass of CH_4 and CO_2, respectively;
h	reservoir thickness, m;
w_h	hydraulic fracture width, m;
Subscript	
i	the gas species, with i=1 for methane and i=2 for carbon dioxide.
k/m/f/h/c	Represents kerogen cells/matrix system/natural fractures/hydraulic fractures/clay cells.

References

Boosari, S. S. H., U. Aybar and M. O. Eshkalak (2015). Carbon dioxide storage and sequestration in unconventional shale reservoirs. Journal of Geoscience and Environment Protection 3(01): 7.

Cao, P., J. Liu and Y. K. Leong (2017). A multiscale-multiphase simulation model for the evaluation of shale gas recovery coupled the effect of water flowback. Fuel 199: 191-205.

Chen, Z., X. Liao, X. Zhao, X. Feng, J. Zang and L. He (2015). A new analytical method based on pressure transient analysis to estimate carbon storage capacity of depleted shales: A case study. International Journal of Greenhouse Gas Control 42: 46-58.

Edwards, R. W., M. A. Celia, K. W. Bandilla, F. Doster and C. M. Kanno (2015). A model to estimate carbon dioxide injectivity and storage capacity for geological sequestration in shale gas wells. Environmental science & technology 49(15): 9222-9229.

Gallo, Y. L. and T. A. Carballo (2016). Quantitative Assessments of CO2 Injection Risks for Onshore Large Scale CO2 Storage. Spe Europec Featured at Eage Conference and Exhibition.

He, J., W. Teng, J. Xu, R. Jiang and J. Sun (2016). A quadruple-porosity model for shale gas reservoirs with multiple migration mechanisms. Journal of Natural Gas Science and Engineering 33: 918-933.

He, J., W. Teng, J. Xu, R. Jiang and J. Sun (2016). A quadruple-porosity model for shale gas reservoirs with multiple migration mechanisms. Journal of Natural Gas Science & Engineering 33: 918-933.

Heller, R. and M. Zoback (2014). Adsorption of methane and carbon dioxide on gas shale and pure mineral samples. Journal of Unconventional Oil and Gas Resources 8: 14-24.

Javadpour, F. (2009). Nanopores and Apparent Permeability of Gas Flow in Mudrocks (Shales and Siltstone). Journal of Canadian Petroleum Technology 48(8): 16-21.

Javadpour, F., D. Fisher and M. Unsworth (2007). Nanoscale Gas Flow in Shale Gas Sediments. Journal of Canadian Petroleum Technology 46(10): 55-61.

Jiang, J., Y. Shao and R. M. Younis (2014). Development of a multi-continuum multi-component model for enhanced gas recovery and CO2 storage in fractured shale gas reservoirs. SPE improved oil recovery symposium, Society of Petroleum Engineers.

Kang, S. M., E. Fathi, R. J. Ambrose, I. Y. Akkutlu and R. F. Sigal (2011). Carbon dioxide storage capacity of organic-rich shales. Spe Journal 16(04): 842-855.

Kim, T. H., J. Cho and K. S. Lee (2017). Evaluation of CO 2 injection in shale gas reservoirs with multi-component transport and geomechanical effects. Applied Energy 190: 1195-1206.

Li, L. and S. Lee (2008). Efficient Field-Scale Simulation of Black Oil in a Naturally Fractured Reservoir via Discrete Fracture Networks and Homogenized Media. Spe Reservoir Evaluation & Engineering 11(4): 750-758.

Liu, M., C. Xiao, Y. Wang, Z. Li, Y. Zhang, S. Chen and G. Wang (2015). Sensitivity analysis of geometry for multi-stage fractured horizontal wells with consideration of finite-conductivity fractures in shale gas reservoirs. Journal of Natural Gas Science & Engineering 22: 182-195.

Merey, S. and C. Sinayuc (2016). Analysis of carbon dioxide sequestration in shale gas reservoirs by using experimental adsorption data and adsorption models. Journal of Natural Gas Science and Engineering 36: 1087-1105.

Moinfar, A., A. Varavei, K. Sepehrnoori and R. T. Johns (2014). Development of an Efficient Embedded Discrete Fracture Model for 3D Compositional Reservoir Simulation in Fractured Reservoirs. Spe Journal 19(2): 289-303.

Pruess, K. (2010). GMINC-A mesh generator for flow simulations in fractured reservoirs. Lawrence Berkeley National Laboratory.

Pruess, K. and T. Narasimhan (1982). A practical method for modeling fluid and heat flow in fractured porous media.

Sun, H., J. Yao, S.-h. Gao, D.-y. Fan, C.-c. Wang and Z.-x. Sun (2013). Numerical study of CO 2 enhanced natural gas recovery and sequestration in shale gas reservoirs. International Journal of Greenhouse Gas Control 19: 406-419.

Svrcek, W. Y. and A. K. Mehrotra (1982). Gas solubility, viscosity and density measurements for Athabasca bitumen. Journal of Canadian Petroleum Technology 21(04).

Swami, V. and A. Settari (2012). A pore scale gas flow model for shale gas reservoir. SPE Americas Unconventional Resources Conference, Society of Petroleum Engineers.

Warren, J. and P. J. Root (1963). The behavior of naturally fractured reservoirs.

Weniger, P., W. Kalkreuth, A. Busch and B. M. Krooss (2010). High-pressure methane and carbon dioxide sorption on coal and shale samples from the Paraná Basin, Brazil. International Journal of Coal Geology 84(3-4): 190-205.

Wilke, C. R. (1950). A Viscosity Equation for Gas Mixtures. Journal of Chemical Physics 18(4): 517-519.

Wu, M., M. Ding, J. Yao, S. Xu, L. Li and X. Li (2017). Pressure transient analysis of multiple fractured horizontal well in composite shale gas reservoirs by boundary element method. Journal of Petroleum Science & Engineering 162.

Wu, Y.-S., G. J. Moridis, B. Bai and K. Zhang (2009). A multi-continuum model for gas production in tight fractured reservoirs. SPE Hydraulic Fracturing Technology Conference, Society of Petroleum Engineers.

Xiao, C., L. Tian, Y. Yang, Y. Zhang, D. Gu and S. Chen (2016). Comprehensive application of semi-analytical PTA and RTA to quantitatively determine abandonment pressure for CO 2 storage in depleted shale gas reservoirs. Journal of Petroleum Science & Engineering 146: 813-831.

Xu, R., K. Zeng, C. Zhang and P. Jiang (2017). Assessing the feasibility and CO 2 storage capacity of CO 2 enhanced shale gas recovery using Triple-Porosity reservoir model. Applied Thermal Engineering 115: 1306-1314.

Zhu, G. P., J. Yao, H. Sun, M. Zhang, M. J. Xie, Z. X. Sun and T. Lu (2016). The numerical simulation of thermal recovery based on hydraulic fracture heating technology in shale gas reservoir. Journal of Natural Gas Science & Engineering 28: 305-316.

- Developing a multi-continuum quadruple porosity binary component gas model
- Considering multiple flow mechanisms for binary component gas
- Solving this model by finite difference method and quasi-Newton iterative method
- Estimating CO_2 storage capacity and CO_2 enhanced shale gas recovery
- Simulating fracture-matrix transfer flow by modified multiple interacting continua method